Field Controlled Magnetisation Patterns in Three-Arm Star Shaped Nanoparticles as Prototypes of Reconfigurable Routing and Vortex State Memory Devices

Dominika Kużma *, Piotr Zegan, Yaroslav Parkhomenko, Piotr Zieliński *

Posted Date: 22 December 2025

doi: 10.20944/preprints202512.1977.v1

Keywords: magnetic nanoparticles; self-similarity; vortices; triple valves; logic devices

 doi:10.20944/preprints202512.1977.v1

Article

Field Controlled Magnetisation Patterns in Three-Arm Star Shaped Nanoparticles as Prototypes of Reconfigurable Routing and Vortex State Memory Devices

Dominika Kuźma [1,*], Piotr Zegan [2], Yaroslav Parkhomenko [2] and Piotr Zieliński [1,*]

[1] Institute of Nuclear Physics Polish Academy of Sciences, PL-31342 Krakow, Poland

[2] Faculty of Materials Science and Physics, Cracow University of Technology, ul. Podchorążych 1, 30-084 Kraków, Poland

* Correspondence: dominika.kuzma@ifj.edu.pl (D.K.); piotr.zielinski@ifj.edu.pl (P.Z.)

Abstract

A model of nanoparticles has been designed to resemble partly self-similar ferroelastic star-like domain textures. Numerical computations have been used to find the equilibrium configurations of magnetisation in such systems. As expected from symmetry, the self-similar initial states give room to other types of domain structure as a function of the star parameters. When relaxed without external field the self-similar pattern mostly turns to a massive vortex in the center with radially oriented domains in the peripheral arms of the star. In contrast to that a random initial state ends up in a configuration of a triple valve with one input and two outputs or vice versa in analogy to logical gates. A treatment with an in-plane magnetic field always leads to the valve configuration. The triple-valve states turn out stable and the vortex ones metastable. The results may be useful in the design of magnetic based logic devices.

Keywords: magnetic nanoparticles; self-similarity; vortices; triple valves; logic devices

1. Introduction

Triple magnetic junctions are promising in development of more efficient and energetically economic logic systems [1,2]. An important issue in this field is the appropriate design of domain walls and a facility in an external stirring of their arrangement [3,4]. The magnetic order, in particular formation of vortices, is essential in the performance of magnetic logic gates [5,6]. The use of magnetic nanoparticles and/or nanodots [7] showing a strong sensitivity and directly detectable variations of their magnetic state is desirable in manufacturing of magnetic switches and sensors [7–9]. Elucidative examples of triple geometry can be found in natural systems. In particular three-arm star patterns of ferroic domains are encountered in a number of systems in which a phase transition involves a loss of three-fold or six-fold crystallographic axis [10–14]. The ferroelastic star patterns show resemblance to triple junctions ubiquitous in the logic devices. Magnetic analogues of electronic structures are now extensively studied in view of reduction of electron leakage and energy consumption [15]. Various arrangements of magnetic domain walls, vortices and fan-out gates etc. have been considered [16–18].

In the case of ferroelastics, the mechanism of formation of the triple star patterns is somewhat different depending whether the low-symmetry phase is orthorhombic or monoclinic and whether one of the preserved axes stays parallel to the initial three-fold axis [15]. When the latter is not the case an arm of the star consists of a twinned pair of ferroelastic domains [16]. The frames of the star are planar domain walls specific to ferroelastic phase transitions. In principle the system prefers

 doi:10.20944/preprints202512.1977.v1

stress-free orientations of domain walls predictable from the decomposition of the point group of the high-symmetry phase into left costs of its low-symmetry subgroup. New energetic conditions occur, however, when the ideal stress-free domain walls intersect forming lines parallel to the initial 3-fold axis. The traces of these lines in the plane perpendicular to the triple axis can be treated as nodes with different number of outgoing branches, i.e., traces of the domain walls. It has been shown [19] that every such node, except for one, generates a stress, due to a disclination when the spontaneous strain of the ferroic phase departs from zero. The exceptional stress-free, or zero-disclination, node consists of two opposite sectors of a domain, say V_I, one sector containing five and the other one approximately 30° large segments, the rest of the space is filled with two remaining domains V_{II} and V_{III} whose angular extent is about 3 x 30° = 90°. The node has been given name (3,1,3,5) [19], that refers to the extent of the sectors, and shown to rest stress-free independently of the actual value of the spontaneous strain. The actual value of strain determines the exact extent of the angles. It is by nesting such nodes that the three-arm stars come into being. This mechanism has been shown in Figure S15 of ref. [13] (Supporting information). To preserve the (3,1,3,5) structure the star nests one within another which gives rise to a several levels of self-similarity, in that an outer star is an image of its inner predecessor by a homothety with the scaling factor determined by the actual extent of the angles. A particularly rich star-like patterns have been recently observed in organic-inorganic hybrid [13]. Some of the phases involved are ferroelectric. The use of the ferreoelastic and ferroelectric triple elements in the logic devices deserves further studies. Here we show some results for system of analogous geometry consisting of magnetic isotropic materials.

In the present paper, we study triple structures filled with ferromagnetic domains as possible prototypes of magnetic logic devices and switch sensors. The analogy of magnetic and ferroelastic structures is all the more pronounced that some materials studied in [13] are ferroelectric. Contrary, however, to the materials studied in ref. [13] where the spontaneous electric polarisation is parallel to the generic triple axis, we impose here the magnetisation in the plane of the star which is one of possible choices giving rise to potentially three input or output paths for the magnetic flux as it is encountered in logic devices. The basic geometry of the star-like magnetic particle is depicted in Figure 1 for a particular choice of angle $\varphi = 30°$ ($\theta = 150°$) corresponding to the ideal ferroelastic case. This geometry allows us to make use of the shape anisotropy created by the acute arms of the star. The gradually narrowing arms tend to align the magnetisation along their axes, even if the material itself does not show a magnetocrystalline anisotropy. We verify the expectations derived from the ferroelastic patterns with numerical modelling performed using the software MuMax3. It allows us to find the equilibrium stable or metastable configurations as functions of the applied external field. The details of the model, particularities of the geometry, selection of material and computation techniques are outlined in Section 2. Section 3 presents relaxed patterns obtained without and with an external magnetic field for various initial configurations to reveal the impact of an initial self-similarity on the stable or metastable magnetic configurations. The treatment with magnetic field allows us to predict the switching mechanisms of the system under study. The angular parameters of the star turn out crucial for the coercivity and switching performance of the particles. Section 4 summarizes the observations made and states suggestions of their practical applications.

2. Materials and Methods

The geometry of a magnetic star inspired by the similar shapes in ferroelastic species is schematized in Figure 1. The panel (a) illustrates carving of the magnetic region (black) on the background of a non-magnetic surrounding (blue). Such a star shows a symmetry of the 2D dihedral point group 3m (D3) and is parametrised with an angle φ or equivalently $\theta = \varphi + 120°$ marked in the Figure. In the ideal geometry corresponding to a vanishing spontaneous strain in the ferroelastic material [13] the angle $\varphi = 30°$ or $\theta = 150°$. In Figure 1(a) one sees how the black star is carved out of an equilateral blue triangle; three similar isosceles triangles of an angle θ are removed from the initial triangle.

 doi:10.20944/preprints202512.1977.v1

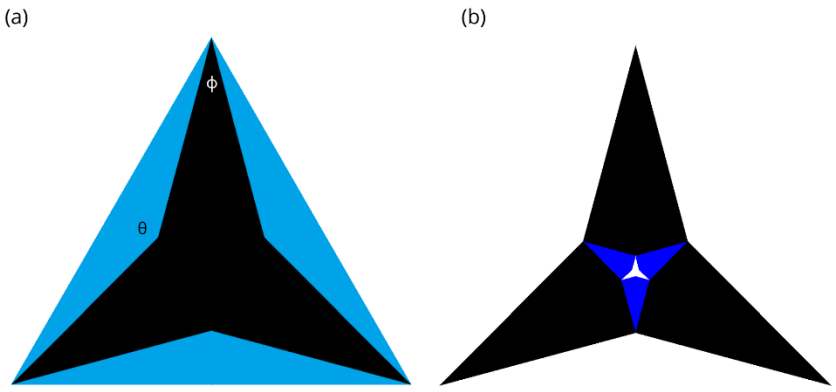

Figure 1. (a) Geometry of carving a star-like particle and (b) schematic of introducing self-similarity.

The scheme of Figure 1(b) is constructed so that the angles delineating the kite-like deltoidal regions of the same colour correspond to those the node (3,1,3,5) [19] of the ideal ferroelastic case. The innermost white region in Figure 1(b) is a core which constitutes a limit of the self-similarity or the first generation of refs. [13 and 20]. Indeed, the scaling invariance cannot descend below the atomic scale in any real material. Therefore, the smallest star must exist as an generic level or the first generation of self-similarity[20].

The fundamental difference between the ferreoelastic and the present case is now that the imposed magnetisation laying in the plane of the particle exhibits pseudovectorial (antisymmetric second rank tensor) nature in contrast with strain which is a symmetric second rank tensor. The pseudovector, when reflected in a plane perpendicular to it, can be oriented in two opposite directions, whereas the opposite directions are equivalent for the strain. Consequently, an initial self-similar state may be prepared in two different manners schematized in Figure 2.

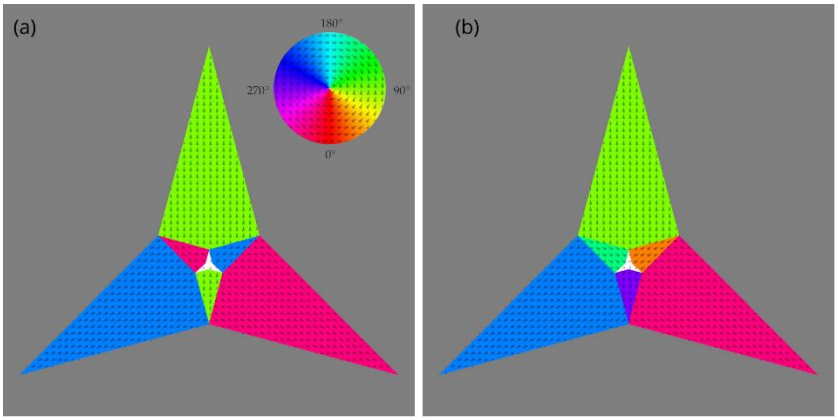

Figure 2. Two self-similar arrangements of magnetisation in the geometry of three-arm star. (a) involving 3 domains (b) involving 6 domains. The orientation of magnetisation is represented with colours according to the colour circle of the software MuMax3 shown in the inset. The direction of arrows is correlated with colours. Red: horizontal right, green: vertical upwards, cyan: horizontal left, violet: vertical downwards [21].

The arrangement of Figure 2(a) involves three orientations of magnetisation aligned along the axes of the arms of the star. The magnetisation in the oppositely oriented arms belonging to consecutive generations of self-similarity is the same or is rotated by 180° as the pseudovector does not change under this rotation. The number of the imposed domains is, therefore, 3 as it is the case in the ferroelastic material. In contrast to that, the arrangement of Figure 2(b) shows opposite magnetisation in the oppositely directed arms, i.e., the magnetisations of oppositely oriented arms of subsequent generations are their mutual images in the mirror plane perpendicular to the so related arms. The number of colours is now 6, violet representing the direction opposite to green, orange to

 doi:10.20944/preprints202512.1977.v1

blue and cyan to magenta. In what follows we will call the configurations of Figure 2(a) and 2(b) 3-domain and 6-domain configurations, respectively.

The initial magnetic configurations do not a priori correspond to a minimum of energy, i.e., they are not equilibrium states. In what follows we study the impact of the initially prepared self-similar arrangements on the closest stable or metastable magnetic state. We use the software MuMax3 [22–24] to relax the system to the corresponding equilibrium states. An advantage of this software is that it implies a well-defined size of voxels, here 2 nm x 2 nm x 2 nm. It bears an analogy to the natural materials in which the scale cannot be fine-grained beyond the atomic size limit. Noteworthy is that the same limitation is in power in the ferroelastic case which, all that withstanding, shows quite a number of self-similarity levels. The size of the largest triangle of Figures 1 and 2 is such that the vertical and horizontal dimensions of the outer square marked with gray are 1000 x 1000 voxels. The height of the largest triangle, thus, amounts to 800 voxels. The thickness of the system is held constantly 5 voxels. We have checked that with this thickness the magnetisation is always uniform across the dimension perpendicular to the image plane.

The simulations reproduce physical behaviour of the coarse grained magnetization $\boldsymbol{M}$ subjected to a local magnetic field $\boldsymbol{H}_{eff}$ resulting from the field applied from outside and one produced by the neighbouring voxels. The magnetization then obeys the Landau–Lifshitz–Gilbert (LLG) equation

$$\frac{d\mathbf{M}}{dt} = -\gamma\left(\mathbf{M}\times\mathbf{H}_{\boldsymbol{eff}} - \eta\mathbf{M}\times\frac{d\mathbf{M}}{dt}\right), \quad (1)$$

where γ is the electron gyromagnetic ratio and η is a phenomenological damping parameter [25]

Our simulations are performed quasi-statically i.e., consist in finding a minimum of magnetic energy starting from an initial configuration, without however, taking into account inertial effects of spin rotations that may happen in real systems as results of sudden changes of external field or of the configuration of neighbouring spins. Out of the operation modes offered by the software MuMax3 [22–24] we use the *relax* one in finding the equilibrium configurations without external field (Section 3.1.). The magnetic moments of the voxels then evolve according to the Landau-Lifshitz-Gilbert (LLG) equation (1) with a defined damping constant. Apart from the study without external field (Section 3.1.) and at the first stage of modelling for the extreme value of the external field B = 1000 mT, where the system searches its equilibrium state after being put into an initial saturated configuration with all the voxel moments aligned with the external field (Section 3.2.). The dimensionless damping factor in the LLG equation then amounts to 0.02. In the study with variating external field the field is swept from +1000 mT to -1000 mT with an increment of 1 mT. The mode *minimize* of MuMax3 is then employed. This search for a minimum of energy enhanced by the conjugate gradient method [26] with an extreme damping that makes the motion of the magnetic moments equivalent to a wandering on the energy map. The simulation is stopped when the maximal unitless torque normalised specifically to the MuMax3 software becomes smaller than 10^{-6} [27]. The procedure corresponds to a physical precessional motion of magnetic moments, however slowed down to zero by an extremely large damping constant in the Landau-Lifshitz-Gilbert equation [28].

The material under study here is Permalloy, i.e., an isotropic magnet whose saturation magnetisation is $M_s = 800\frac{kA}{m}$ and the exchange interaction constant amounts to $A_{ex} = 1.3\times 10^{-11}\frac{J}{m}$ [29,30]. The only source of anisotropy, therefore, is the shape anisotropy. This seems an appropriate choice for the first reference study.

3. Results

To reveal the behaviour of the system in different conditions we show below results in zero external field starting from self-similar and random configurations and, afterwards, under a uniaxial variating magnetic field. The parameters $\theta = 120° + \varphi$ of the stars have been selected so as to cover the region from the most acute star to the limit in which it becomes equivalent to an equilateral triangle. This is presented in Figure 3. The tightest angle φ allowing one to model a triangle with its

 doi:10.20944/preprints202512.1977.v1

apex consisting of a single voxel (and not a 1D chain of voxels attached to the apex, which would introduce a different geometry) amounts to $\varphi = 6°$, so that $\theta = 126°$.

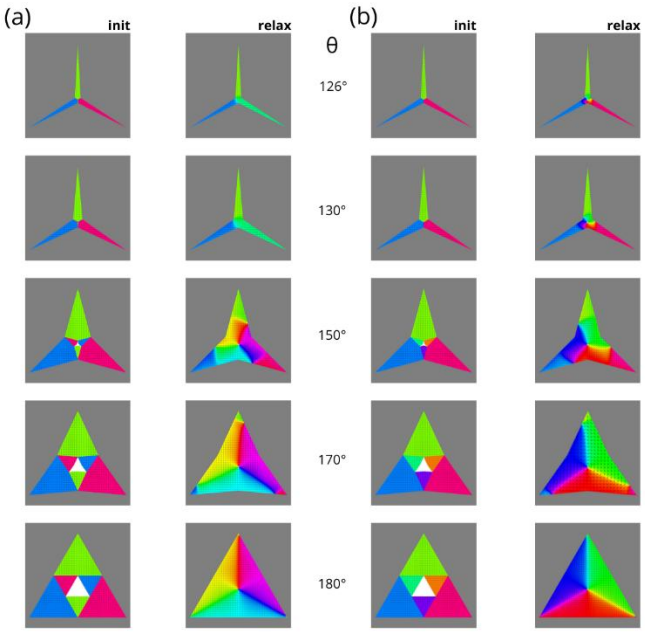

Figure 3. Relaxation of the 3- and 6-domain self-similar configurations (see Figure 2) for 5 angles θ marked in the middle in degrees. In column (a) the starting point is 3-domain and in column (b) 6-domain.

3.1. Non Biased Paths to Equilibrium States

The first series of studies is done without any external field. This allows one to watch the configurations to which the initial 3- and 6-domain partly self-similar patterns defined in Figure 2 wander spontaneously without any symmetry-breaking perturbation as functions of the angle θ. The angle turns out to be crucial in qualitative determination of the final state. Some examples are shown in Figure 3.

The white innermost star in the initial states contains spins directed perpendicularly to the surface towards the viewer in accordance with the colour code of the software MuMax3. This choice has been made to avoid any initial bias for the in-plane magnetic moments. It also turns out a good guess because an upward spot, although reduced in size, is present in all the relaxed configurations independently of initial conditions. The spot has been found to be a concomitant of a vortex [31].

Whereas the 6-domain commencing leads systematically to a central vortex, in the 3-domain initial state the vortex seems to be hindered by narrow arms (126° and 130°) and appears for θ larger than 150°. The radial extent of the vortex is limited to the central part of the, star whereas the peripheral apices mainly remain in their initial radially divergent configurations. The vortex is always separated from the radially oriented parts with kind of domain walls. The walls are not straight and their lateral extent varies along their lengths. The phenomenon is more pronounced for the 6-domain initial configurations. E.g. for 150° the domain wall separating the vortex from the green area of the vertical arm is quite sharp on the left hand border of the arm and separates regions differing by 60° whereas it is diffused, if non-existent at all, on the right hand border, where the green colour dominates on both sides. In the column a) of Figure 3 the walls are much more sharp on all their lengths. An example of this kind of behaviour is provided in Figure 4. Noteworthy is that the chirality of the vortices with 3 and 6 initial domains is opposite; the white spot in the centre points always upwards, but the circulations of the magnetic moments are opposite.

 doi:10.20944/preprints202512.1977.v1

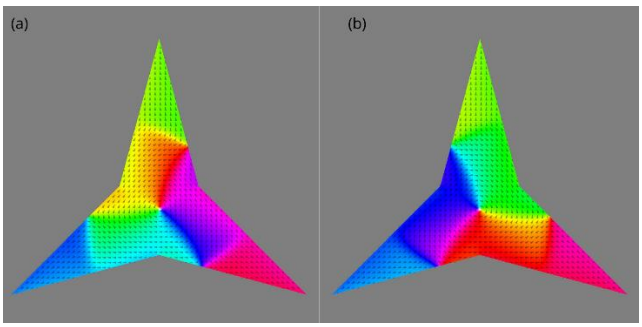

Figure 4. Magnification of relaxed vortices of Figure 3 for θ = 150°.

In the cases of the most narrow arms (θ = 126° and 130°) the system ends up in a different configuration deprived of a central vortex. The final configurations then resemble a three-wave valve, router or a logical gate in that the two arms are orientedout of the centre and one into the centre of the star. Thus two arms play a role of outputs and the third reversed one becomes an input. This is achieved by a quasi 180° reorientation of one of the arms, see the lower right arms in Figure 3 (a) for 126° and 130°. In contrast to that the configurations involving 6 initial domains always evolve towards a vortex in the center of the star.

A comparison of energies of the most narrow stars (θ = 126° and 130°), reveals that the triple-valve configurations are more stable (Figure 3(a)) that vortex ones (Figure 3(b)) in that the energies of the former are about 3 times smaller than of the latter. On the other hand, the energies of the vortex states for θ = 150°, 170° and 180° are equal to 5 significant figures in spite of geometric differences.

A study with totally random initial configuration turns out much more time-consuming. Generally such simulations favour the triple valve final state. Figure 5 shows both the initial and the final states for θ = 150°.

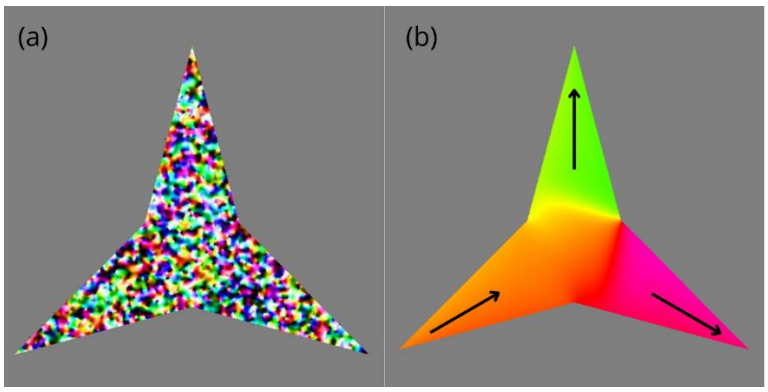

Figure 5. Relaxation of totally random (in-plane and out-of-plane) initial configuration at θ = 150°.

The final stage is clearly the logical gate with one input and two output arms. The domain of the input arm shows a very regular deltoid shape limited with somewhat curved domain walls. This is in a correspondence with the geometry of the node (3,1,3,5) [13]. The energy of this triple valve turns out almost four times lower as compared with the energy of the vortex states of Figure 4.

3.2. Switching Properties and Equilibrium States Under an External Field

A treatment with an external magnetic field may cast a light on the most efficient method of fabrication of configurations useful for technological applications. A series of such studies are depicted in Figure 6 for 5 angles θ defining the geometry of the star: 180°,170°, 150°, 130° and 126°. The external field is applied vertically, i.e., along the axis of the upward arm. The initial value of the field is 1000 mT. It practically ensures a complete bias upwards for θ = 180° but more acute stars relax to slightly inhomogeneous states at this field as it follows from the application of the *relax* operational

 doi:10.20944/preprints202512.1977.v1

mode of MuMax3. The field is decreased at 1 mT increment down to -1000 mT. This protocol allows us to satisfy conditions of adiabaticity and to study a complete switching of the particles. Recording of the net magnetisation in the vertical (y) direction provides the corresponding hysteresis loops. They turn out to be symmetric. Therefore, only the parts of hysteresis loops obtained with decreasing field are shown in Figure 6(a) for clarity.

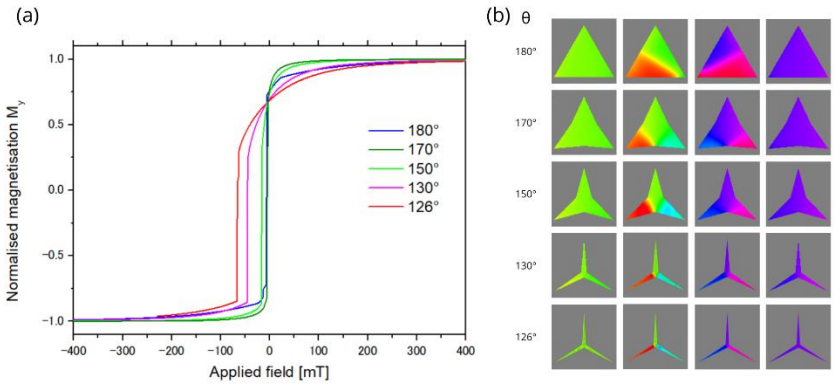

Figure 6. (a) Half-loops of hysteresis corresponding to decreasing field for the stars specified in the column θ. (b) initial states (B=1000 mT), the states just before and just after switching and the reversed states of the stars at B= - 1000 mT.

The coercive field increases with decreasing angle θ and is the largest for the most acute stars. The remagnetisation starts with reorientation of spins in the armes situated at the angle 120° with respect to the applied field. The reorientation initiates in the apices of the arms and spreads out to the centre of the star. As a result, a configuration of triple valve "two in - one out" forms before the step-like reversal of the vertical arm. This jump reverses the magnetisation in all three arms so that a triple valve "one in – two out" comes into being being which further becomesd progressively saturated. Apart from step like-jumps the hysteresis loops show rounded parts for the field values where the pattern varies in a continuous way. An exception is the case of the regular triangle at θ = 180° (blue curve in Figure 6(a)), where the progressive expansion of the region coloured in red in Figure 6(b) manifests itself in a slanting straight part preceding the reversal jump. This behaviour manifests the lack of an obstacle imposed by the cusp-like connection of the lower arms when θ ≠ 180°.

The configurations arising after switching off of the field are all of the type triple valve in analogy to those observed for the most acute stars with 3-domain initial state (see Figure 3(a) for θ = 126° and θ = 130°) as well as for the random initial state of Figure 5. The configurations are not identical, however. Their energies when obtained with the field treatment are down to half as high as the ones attained with self-similar and random initial state. Thus, the external filed helps to find the most stable triple valve arrangements.

4. Discussion and Conclusions

The minimisation procedures reported in Section 2 lead to local energy minima which are directly attainable from the prescribed initial states. The minima can, thus, be local or global corresponding to metastable or stable magnetic configurations respectively. The recapitulative Table 1 allows one to compare the energies of the particular relaxed states at B = 0 described in Section 3.

Table 1. Magnetic energy of the relaxed configurations obtained at B = 0 without and with external field treatment. Asterisks indicate vortex states.

E_{tot} [10^{-5} pJ]	3-domain	6-domain	hysteresis	random
180°	2.5278681*	2.5278681*	1.0451257	-
170°	2.9810302*	2.981451*	0.8581696	-

 doi:10.20944/preprints202512.1977.v1

150°	2.9240302*	2.924786*	0.49729887	0.8465562
130°	0.6808681	1.792714*	0.18028585	-
126°	0.51189704	1.3600054*	0.51109695	-

The energies of the vortex states in the 6-domain initial configurations for θ = 126° and θ = 130° are clearly higher than those of the triple-valve type configurations in the 3-domain counterparts. The vortex spin arrangements are, thus, metastable. The self-similar initial configuration of the present systems seems to be a good choice for obtaining vortex states useful in many logic devices [18,32–34]. The chirality of the vortices is clearly determined by whether the initial self-similar configuration is 3-domain or 6-domain. Whereas the 3-domain arrangement favours left-handed helicity, the 6-domain privileges the right-handed one. The fact that the vortex state does not arise in the most acute 3-domain stars indicates that the 6-domain initial state better stimulates the circulating magnetic flux against the triple-valve.

Both types of arrangement in magnetic nanoparticles and their systems are now extensively studied as potential elements of memory and logic devices [35–40]. Their design should be based on the predictable patterns of magnetisation and their liability to external stirring by magnetic fields and other stimuli. The geometry of triple junctions is of special interest in this context because it underlies the functionality of logic gates and transistors [15,16,41]. This geometry has been encountered in the ferroelastic domain textures [11,13,19] with an additional property of several levels of scaling invariance or self-similarity. The latter characteristic turns out to exhibit an unexpected robustness with respect of some external perturbations [20]. While not directly transferable to magnetic structures, for symmetry reasons, such geometry has been used here as initial configurations in magnetic particles shaped in to a form of three-arm stars. When relaxed, such initial states have been shown in Section 3 to give rise to metastable vortex configurations widely studied in the logic devices [18,32–34]. In some cases the relaxed pattern, usually stable, corresponds to a triple valve. The treatment with a homogeneous external field uncontestably favours such configurations. The coercivity of the magnetic elements is also an important factor for technology, especially when the memory storage devices are considered. In the case of our three-arm stars the coercive field increases with the acuity of stars. This indicates the effective modalities for fabrication of magnetic configurations desired for specific application.

Author Contributions: Conceptualization, D.K. and P.Z.[1]; methodology, D.K. and P.Z.[1]; software, D.K.; investigation, D.K., P.Z.[2], Y.P. and P.Z.[1]; data curation, D.K.; writing—original draft preparation, D.K., P.Z.[2], Y.P. and P.Z.[1]; writing—review and editing, D.K., P.Z.[2], Y.P. and P.Z.[1]; visualization, D.K.; supervision, P.Z.[1]; funding acquisition, D.K. All authors have read and agreed to the published version of the manuscript.

Funding: We gratefully acknowledge Polish high-performance computing infrastructure PLGrid (HPC Center: ACK Cyfronet AGH) for providing computer facilities and support within computational grant no. PLG/2024/017851.

Institutional Review Board Statement: Not applicable.

Informed Consent Statement: Not applicable.

Data Availability Statement: Data will be made available on request.

Acknowledgments: We gratefully acknowledge Polish high-performance computing infrastructure PLGrid (HPC Center: ACK Cyfronet AGH) for providing computer facilities and support within computational grant no. PLG/2024/017851.

Conflicts of Interest: The authors declare no conflicts of interest.

 doi:10.20944/preprints202512.1977.v1

References

1. Chen, Z.; Lin, T.-Y.; Wei, X.; Matsunaga, M.; Doi, T.; Ochiai, Y.; Aoki, N.; Bird, J.P. The Magnetic Y-Branch Nanojunction: Domain-Wall Structure and Magneto-Resistance. *Appl. Phys. Lett.* **2012**, *101*, 102403, doi:10.1063/1.4750240.
2. Currivan-Incorvia, J.A.; Siddiqui, S.; Dutta, S.; Evarts, E.R.; Zhang, J.; Bono, D.; Ross, C.A.; Baldo, M.A. Logic Circuit Prototypes for Three-Terminal Magnetic Tunnel Junctions with Mobile Domain Walls. *Nat Commun* **2016**, *7*, 10275, doi:10.1038/ncomms10275.
3. Saxena, V.; Gutzeit, M.; Rodríguez-Sota, A.; Haldar, S.; Zahner, F.; Wiesendanger, R.; Kubetzka, A.; Heinze, S.; Von Bergmann, K. Strain-Driven Domain Wall Network with Chiral Junctions in an Antiferromagnet. *Nat Commun* **2025**, *16*, 10808, doi:10.1038/s41467-025-66700-0.
4. Alamdar, M.; Leonard, T.; Cui, C.; Rimal, B.P.; Xue, L.; Akinola, O.G.; Patrick Xiao, T.; Friedman, J.S.; Bennett, C.H.; Marinella, M.J.; et al. Domain Wall-Magnetic Tunnel Junction Spin–Orbit Torque Devices and Circuits for in-Memory Computing. *Applied Physics Letters* **2021**, *118*, 112401, doi:10.1063/5.0038521.
5. Bhattacharjee, P.; Barman, S. Three-Input Magnetic Logic Gates Using Magnetic Vortex Transistor. *Physica Status Solidi (a)* **2022**, *219*, 2200397, doi:10.1002/pssa.202200397.
6. Anisul Haque, S.; Yamamoto, M.; Nakatani, R.; Endo, Y. Binary Logic Gates by Ferromagnetic Nanodots. *Journal of Magnetism and Magnetic Materials* **2004**, *282*, 380–384, doi:10.1016/j.jmmm.2004.04.088.
7. Koh, I.; Josephson, L. Magnetic Nanoparticle Sensors. *Sensors* **2009**, *9*, 8130–8145, doi:10.3390/s91008130.
8. Sensing Magnetic Nanoparticles. In *Magnetic Nanoparticles in Biosensing and Medicine*; Darton, N.J., Ionescu, A., Llandro, J., Eds.; Cambridge University Press, 2019; pp. 172–227 ISBN 978-1-139-38122-2.
9. Jia, F.; Xu, L.; Yan, W.; Wu, W.; Yu, Q.; Tian, X.; Dai, R.; Li, X. A Magnetic Relaxation Switch Aptasensor for the Rapid Detection of Pseudomonas Aeruginosa Using Superparamagnetic Nanoparticles. *Microchim Acta* **2017**, *184*, 1539–1545, doi:10.1007/s00604-017-2142-2.
10. Manolikas, C.; Amelinckx, S. Phase transitions in ferroelastic lead orthovanadate as observed by means of electron microscopy and electron diffraction. I. Static observations. *Phys. Stat. Sol. (a)* **1980**, *60*, 607–617, doi:10.1002/pssa.2210600233.
11. Boulesteix, C.; Yangui, B. Star patterns and dissociation of interfaces without spontaneous strain compatibility between orientation domains in ferroelastic crystals. Case of a monoclinic rare earth sesquioxide. *Phys. Stat. Sol. (a)* **1983**, *78*, 303–308, doi:10.1002/pssa.2210780136.
12. Curnoe, S.H.; Jacobs, A.E. Statics and Dynamics of Domain Patterns in Hexagonal-Orthorhombic Ferroelastics. *Phys. Rev. B* **2001**, *63*, 094110, doi:10.1103/PhysRevB.63.094110.
13. Krupińska, A.; Burzyńska, B.; Kinzhybalo, V.; Dziuk, B.; Szklarz, P.; Kajewski, D.; Zaręba, J.K.; Drwęcka, A.; Zelewski, S.J.; Durlak, P.; et al. Ferroelectricity, Piezoelectricity, and Unprecedented Starry Ferroelastic Patterns in Organic–Inorganic $(CH_3C(NH_2)_2)_3[Sb_2X_9]$ (X = Cl/Br/I) Hybrids. *Inorg. Chem.* **2025**, *64*, 9639–9651, doi:10.1021/acs.inorgchem.5c00667.
14. Vicens, J.; Delavignette, P. A Particular Domain Configuration Observed in a New Phase of the Ta⊙N System. *Phys. Stat. Sol. (a)* **1976**, *33*, 497–509, doi:10.1002/pssa.2210330208.
15. Bhattacharjee, P.; Barman, A.; Barman, S. Operation of Magnetic Vortex Transistor by Spin-Polarized Current: A Micromagnetic Approach. *Physica Status Solidi (a)* **2022**, *219*, 2100564, doi:10.1002/pssa.202100564.
16. Omari, K.A.; Hayward, T.J. Chirality-Based Vortex Domain-Wall Logic Gates. *Phys. Rev. Applied* **2014**, *2*, 044001, doi:10.1103/PhysRevApplied.2.044001.
17. Gypens, P.; Van Waeyenberge, B.; Di Ventra, M.; Leliaert, J.; Pinna, D. Nanomagnetic Self-Organizing Logic Gates. *Phys. Rev. Applied* **2021**, *16*, 024055, doi:10.1103/PhysRevApplied.16.024055.
18. Hertel, R.; Gliga, S.; Fähnle, M.; Schneider, C.M. Ultrafast Nanomagnetic Toggle Switching of Vortex Cores. *Phys. Rev. Lett.* **2007**, *98*, 117201, doi:10.1103/PhysRevLett.98.117201.
19. Kitano, Y.; Kifune, K.; Komura, Y. STAR-LISCLINATION IN A FERRO-ELASTIC MATERIAL B19 MgCd ALLOY. *J. Phys. Colloques* **1988**, *49*, C5-201-C5-206, doi:10.1051/jphyscol:1988520.
20. Sobieszczyk, P.; Mroczek, M.; Kuźma, D.; Zieliński, P. Negative Mechanical Characteristics of Self-Similar Star-Like Hinged Grilles. *Physica Status Solidi (b)* **2024**, *261*, 2400399, doi:10.1002/pssb.202400399.

 doi:10.20944/preprints202512.1977.v1

21. Kuźma, D.; Pastukh, O.; Zieliński, P. Competing Magnetocrystalline and Shape Anisotropy in Thin Nanoparticles. *Crystals* **2024**, *14*, 375, doi:10.3390/cryst14040375.
22. Vansteenkiste, A.; Leliaert, J.; Dvornik, M.; Helsen, M.; Garcia-Sanchez, F.; Waeyenberge, B.V. The Design and Verification of MuMax3. *AIP Advances* **2014**, *4*, 107133, doi:10.1063/1.4899186.
23. Leliaert, J.; Dvornik, M.; Mulkers, J.; De Clercq, J.; Milošević, M.V.; Van Waeyenberge, B. Fast Micromagnetic Simulations on GPU—Recent Advances Made with mumax^3. *J. Phys. D: Appl. Phys.* **2018**, *51*, 123002, doi:10.1088/1361-6463/aaab1c.
24. Moreels, L.; Lateur, I.; De Gusem, D.; Mulkers, J.; Maes, J.; Milošević, M.V.; Leliaert, J.; Van Waeyenberge, B. Mumax+: Extensible GPU-Accelerated Micromagnetics and Beyond 2024.
25. Aharoni, A. *Introduction to the Theory of Ferromagnetism*; 2. ed., repr.; Oxford University Press: Oxford, 2007; ISBN 978-0-19-850809-0.
26. Bouwmeester, H.; Dougherty, A.; Knyazev, A.V. Nonsymmetric Preconditioning for Conjugate Gradient and Steepest Descent Methods 1. *Procedia Computer Science* **2015**, *51*, 276–285, doi:10.1016/j.procs.2015.05.241.
27. Joos, J.J.; Bassirian, P.; Gypens, P.; Mulkers, J.; Litzius, K.; Van Waeyenberge, B.; Leliaert, J. Tutorial: Simulating Modern Magnetic Material Systems in Mumax3. *Journal of Applied Physics* **2023**, *134*, 171101, doi:10.1063/5.0160988.
28. Lifshitz, E.M.; Pitaevskii, L.P.; Pitaevskii, L.P. *Statistical Physics: Theory of the Condensed State*; Course of Theoretical Physics; 3rd ed.; Elsevier Science: Saint Louis, 2013; ISBN 978-0-7506-2636-1.
29. Nahrwold, G.; Scholtyssek, J.M.; Motl-Ziegler, S.; Albrecht, O.; Merkt, U.; Meier, G. Structural, Magnetic, and Transport Properties of Permalloy for Spintronic Experiments. *Journal of Applied Physics* **2010**, *108*, 013907, doi:10.1063/1.3431384.
30. Nguyen, T.M.; Cottam, M.G.; Liu, H.Y.; Wang, Z.K.; Ng, S.C.; Kuok, M.H.; Lockwood, D.J.; Nielsch, K.; Gösele, U. Spin Waves in Permalloy Nanowires: The Importance of Easy-Plane Anisotropy. *Phys. Rev. B* **2006**, *73*, 140402, doi:10.1103/PhysRevB.73.140402.
31. Park, G.; Kim, B.; Kim, S.-K. From Trochoidal Symmetry to Chaotic Vortex-Core Reversal in Magnetic Nanostructures. *npj Spintronics* **2025**, *3*, 42, doi:10.1038/s44306-025-00108-w.
32. Guslienko, K.Yu.; Han, X.F.; Keavney, D.J.; Divan, R.; Bader, S.D. Magnetic Vortex Core Dynamics in Cylindrical Ferromagnetic Dots. *Phys. Rev. Lett.* **2006**, *96*, 067205, doi:10.1103/PhysRevLett.96.067205.
33. Gypens, P.; Leliaert, J.; Schütz, G.; Van Waeyenberge, B. Commensurate Vortex-Core Switching in Magnetic Nanodisks at Gigahertz Frequencies. *Phys. Rev. B* **2022**, *105*, 094420, doi:10.1103/PhysRevB.105.094420.
34. Van Waeyenberge, B.; Puzic, A.; Stoll, H.; Chou, K.W.; Tyliszczak, T.; Hertel, R.; Fähnle, M.; Brückl, H.; Rott, K.; Reiss, G.; et al. Magnetic Vortex Core Reversal by Excitation with Short Bursts of an Alternating Field. *Nature* **2006**, *444*, 461–464, doi:10.1038/nature05240.
35. Kuźma, D.; Laskowski, Ł.; Kłos, J.W.; Zieliński, P. Effects of Shape on Magnetization Switching in Systems of Magnetic Elongated Nanoparticles. *Journal of Magnetism and Magnetic Materials* **2022**, *545*, 168685, doi:10.1016/j.jmmm.2021.168685.
36. Kuźma, D.; Pastukh, O.; Zieliński, P. Spacing Dependent Mechanisms of Remagnetization in 1D System of Elongated Diamond Shaped Thin Magnetic Particles. *Magnetochemistry* **2022**, *8*, 102, doi:10.3390/magnetochemistry8090102.
37. Ding, J.; Kostylev, M.; Adeyeye, A.O. Realization of a Mesoscopic Reprogrammable Magnetic Logic Based on a Nanoscale Reconfigurable Magnonic Crystal. *Appl. Phys. Lett.* **2012**, *100*, 073114, doi:10.1063/1.3687177.
38. Orlov, A.; Imre, A.; Csaba, G.; Ji, L.; Porod, W.; Bernstein, G.H. Magnetic Quantum-Dot Cellular Automata: Recent Developments and Prospects. *Journal of Nanoelectronics and Optoelectronics* **2008**, *3*, 55–68, doi:10.1166/jno.2008.004.
39. Nordquist, K. Process Development of Sub-0.5 Mm Nonvolatile Magnetoresistive Random Access Memory Arrays. *J. Vac. Sci. Technol. B* **1997**, *15*, 2274, doi:10.1116/1.589628.
40. Wu, L.; Jubert, P.-O.; Berman, D.; Imaino, W.; Nelson, A.; Zhu, H.; Zhang, S.; Sun, S. Monolayer Assembly of Ferrimagnetic $Co_xFe_{3-x}O_4$ Nanocubes for Magnetic Recording. *Nano Lett.* **2014**, *14*, 3395–3399, doi:10.1021/nl500904a.

 doi:10.20944/preprints202512.1977.v1

41. Kumar, D.; Barman, S.; Barman, A. Magnetic Vortex Based Transistor Operations. *Sci Rep* **2014**, *4*, 4108, doi:10.1038/srep04108.